Reoxidation of Al-killed Ultra-Low C Steel by Fe_tO in $CaO\text{-}Al_2O_3\text{-}MgO_{sat.}\text{-}Fe_tO$ Slag Representing RH Slag by Experiment and Kinetic Modeling

Y.-M. Cho[1], W.-Y. Cha[2] and Y.-B. Kang[3]

1. Graduate Student, Pohang University of Science and Technology, Pohang, Gyeongbuk, Rep. of Korea, 37673. Email: minn907@postech.ac.kr
2. Senior Researcher, POSCO, Pohang, Gyeongbuk, Rep. of Korea, 37673. Email: chawoo@posco.com
3. Professor, Pohang University of Science and Technology, Pohang, Gyeongbuk, Rep. of Korea, 37673. Email: ybkang@postech.ac.kr

Keywords: $CaO\text{-}Al_2O_3\text{-}MgO_{sat.}\text{-}Fe_tO$, reoxidation, ultra-low C steel, RH process

ABSTRACT

Molten slag used in the secondary refining process (RH process) for the production of Ultra-Low C (ULC) steel is typically composed of $CaO\text{-}Al_2O_3\text{-}MgO_{sat.}\text{-}Fe_tO$ with minor constituents. Fe_tO in the RH slag is the main source of reoxidation of the molten ULC steel in the ladle by $2\underline{Al} + 3(Fe_tO) = (Al_2O_3) + 3Fe$, thereby serving as the source of the alumina inclusions. On the other hand, Fe_tO also enhances the fluidity of the slag, thereby increasing inclusion absorption capacity. Optimum slag chemistry design is therefore required to produce clear ULC steel. The reoxidation kinetics was investigated in the present study by employing high-temperature experiments and developing the reaction rate model. Initial compositions of slag ((pct $CaO)_0$/(pct $Al_2O_3)_0$ and (pct $Fe_tO)_0$)) and reaction temperature were varied, and change of [pct Al] in the molten steel was measured. The rate-controlling step was analysed. It was found that the rate-controlling step in some cases changed during the reoxidation: from a mass transport of Al in the molten steel to a mixed transport including Al_2O_3 in the molten slag. The experimental data validated the reaction rate model based on the elucidated reaction mechanism and FactSage thermodynamic database. The model suggested that high (pct $CaO)_0$/(pct $Al_2O_3)_0$ suppresses the reoxidation only when (pct $Fe_tO)_0$ is low (5 or lower in the present study).

INTRODUCTION

Ultra-Low carbon (ULC) steel is distinguished as clean steel with exceptional formability and ductility, finding application in the production of various structural components for automobiles, necessitating intricate shaping and forming processes. The low carbon content (typically within the range of 10 to 30 mass ppm) in this steel grade makes it susceptible to oxidation during steelmaking and casting procedures. The production of ULC steel involves successive steps, including Blast Furnace (BF), Basic Oxygen Furnace (BOF), Ruhrstahl Heraeus (RH), and Continuous Casting (CC), with reoxidation posing a significant challenge during the RH and CC processes, resulting in the generation of non-metal inclusions (NMI).

ULC steel undergoes deoxidization by Al alloys during the RH process. Once the liquid steel is adequately refined, it proceeds to a casting machine *via* a tundish. Reoxidation during the RH and casting processes can occur due to various factors, such as reactions with the RH slag/tundish flux, open-eye formation in the tundish, reactions with tundish and submerged entry nozzle refractories, and aspiration through the sliding gate (Park and Kang, 2023). Consequently, Al in the liquid steel is depleted, resulting in the production of NMIs, such as alumina. This compromise not only hampers process efficiency but also adversely impacts the quality of the final products.

Narrowing the focus of the present study to reoxidation caused by RH slag reveals that Fe_tO, SiO_2, and MnO may be accountable for this phenomenon. Higher concentrations of these weak oxides can accelerate the reoxidation reaction. Conversely, since the slag absorbs non-metallic inclusions (NMI) at the steel–slag interface, a faster dissolution rate of NMI is necessary. Previous reports have summarised the dissolution rate of alumina inclusion in various slags (Park et al., 2020). Specifically, the dissolution rate of alumina inclusion in Fe_tO-containing RH slag was investigated using a high-

temperature dissolution experimental technique coupled with the modified invariant interface approximation (Feitchtinger et al., 2014). Findings indicate that a decrease in slag viscosity is a key factor in increasing the dissolution rate, aligning with proposals for various slag types. Given that the primary components of RH slag are CaO, Al_2O_3, and Fe_tO, an increase in Fe_tO content ((pct Fe_tO)) would enhance the dissolution rate. However, simultaneously, increasing the (pct Fe_tO) would compromise the cleanliness of the liquid steel. Therefore, a comprehensive understanding of both phenomena – the dissolution of alumina into the RH slag and the reoxidation of the liquid steel by the RH slag – is crucial concerning (pct Fe_tO) in the RH slag. The role of (pct Fe_tO) from a dissolution perspective was recently discussed by the authors (Park et al., 2020).

The present article reports the authors' results that explore the reaction kinetics between ULC-Al killed liquid steel and Fe_tO-containing slag (representing RH slag) through high-temperature chemical reaction experiments and rate model analysis (Cho, Cha, and Kang, 2021). Various rate-controlling steps were considered, compared with experimental data, and a gradual change in the rate-controlling step was highlighted. The study concludes with practical suggestions for RH operation based on these findings.

EXPERIMENTAL PROCEDURE

A series of high-temperature reactions between Fe–Al alloy and CaO–Al_2O_3–$MgO_{sat.}$–Fe_tO slag were carried out, mostly at 1550 °C under a well-controlled atmosphere. The reaction represents an interfacial reaction between Al-killed ULC steel and RH slag. The initial Al content in the liquid steel ([pct Al]$_0$) was set to about 0.1. Nine slag samples were synthesized by melting reagent grade of CaO (calcined from $CaCO_3$), Al_2O_3, and MgO in a graphite crucible. The melt was cooled, crushed, and then burned under air to remove any residual C. Appropriate amount of reagent grade of FeO was then mixed to have various initial compositions of the slag samples: C/A ratio ((pct CaO)$_0$/(pct Al_2O_3)$_0$ and (pct Fe_tO)$_0$ were varied, where $_0$ means the initial state. The initial MgO content ((pct MgO)$_0$) was set to its saturation content, estimated by FactSage FTOxid database (Bale et al, 2016). The initial compositions of the slag samples are listed in TABLE 1. The compositions of the slag and the steel were given in mass pct.

TABLE 1 – Slag compositions used in the present study.

Name	C/A ratio	(pct Fe_tO)$_0$	(pct MgO)$_0$
A5	1.2	5	saturated
A10		10	
A15		15	
B5	1.0	5	
B10		10	
B15		15	
C5	0.8	5	
C10		10	
C15		15	

500 g of Fe-0.01pct Al steel was melted in an induction furnace at 1550 °C, under purified Ar atmosphere. The initial O content in the alloy was approximately 0.002 pct. Then, 40 g of the synthesized slag prepared as above was charged onto the molten steel surface using an alumina guide tube through a hole available in the upper endcap. This moment was set to the beginning of the reaction (t = 0). After the pre-determined time, a small portion of the liquid steel was periodically sampled using a quartz tube, followed by quenching in water. The composition of the liquid steel was analyzed by Inductively Coupled Plasma - Atomic Emission Spectroscopy (ICP-AES) for soluble Al content ([pct. S. Al]) and total Al content ([pct. T. Al]) by inert gas fusion infrared absorptiometry for total O content ([pct. T. O]). The distribution of non-metallic inclusions in the alloy was analyzed using field-emission scanning electron microscopy with an energy-dispersive X-ray spectroscopy. All the data were reported previously (Cho, Cha, and Kang, 2021), and were reproduced in this paper.

EXPERIMENTAL RESULTS

The time evolution of the alloy's composition is shown in FIG 1 for the case of high C/A ratio (= 1.2): [pct. T. Al], [pct. S. Al], [pct T. O] *vs* reaction time *t* (seconds) of liquid steel reacted with slags (A5, A10, and A15) at 1550 °C. Both decreased continuously, and those decreased faster when (pct $Fe_tO)_0$ was higher. The following chemical reaction occurred:

$$2\underline{Al} + 3(FeO) = (Al_2O_3) + 3Fe \quad (1)$$

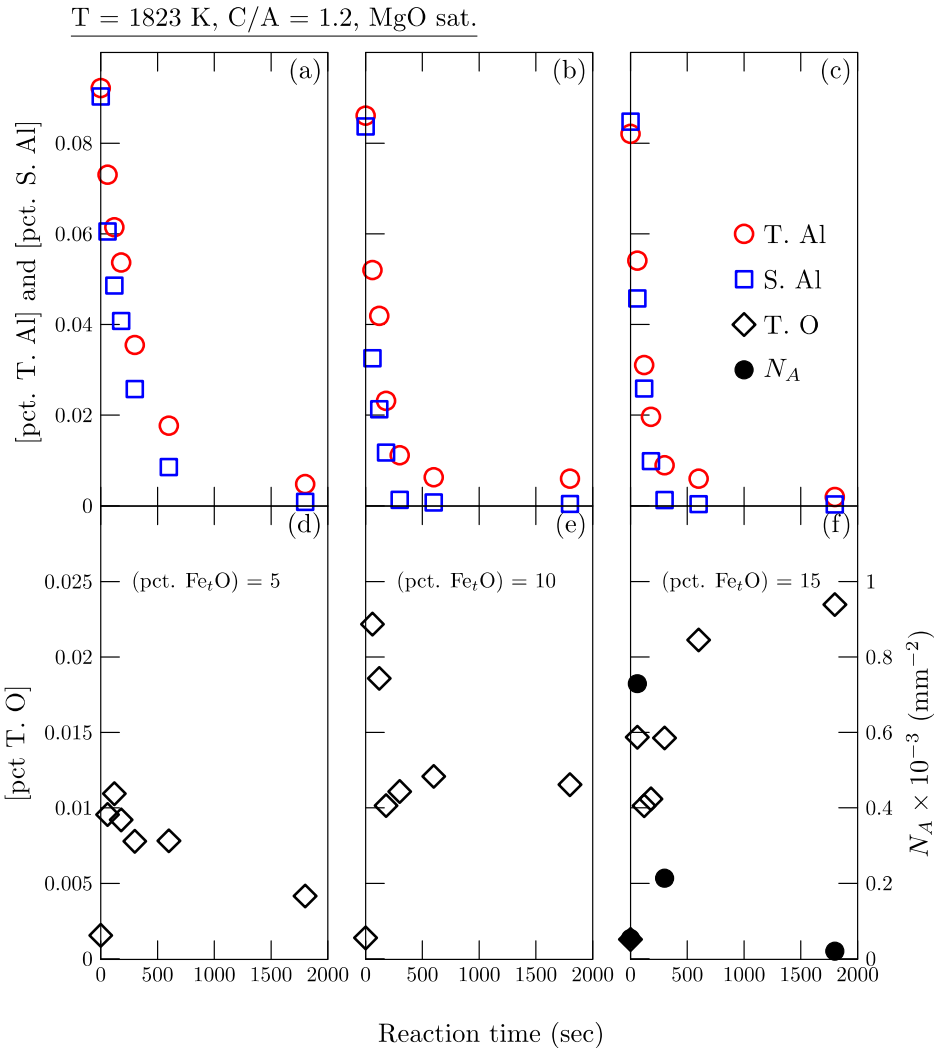

FIG 1 – Composition change of the liquid steel ([pct. Al]$_0$ = 0.1 reacted with $CaO–Al_2O_3–MgO_{sat.}–Fe_tO$ slag): (a) to (c) [pct. T. Al] and [pct. S. Al], (d) to (f) [pct. T. O] of the liquid steel reacted with the slag A5, A10, and A15, respectively, measured in the present study. Closed circles in (f) are the measured inclusion number density N_A, mm^{-2}) (Cho, Cha, and Kang, 2021).

[pct. T. Al] was slightly higher than [pct. S. Al], and the difference should correspond to the insoluble Al content relevant to alumina inclusion in the steel. [pct. T. O] is a sum of soluble O content ([pct. S. O]) and insoluble O content ([pct. I. O]) where the latter corresponds to the O content relevant to alumina inclusion in the steel. Although a simultaneous analysis technique of [pct. S. O] and [pct. I. O] in Al-killed steel was recently developed (Hong and Kang, 2021), it was not attempted in the present study. Therefore, the measured [pct. T. O] should be treated carefully. When (pct $Fe_tO)_0$ = 5, [pct. T. O] first increased, showed a maximum, then decreased. It was thought that (Al_2O_3) in Reaction (1) was mostly alumina inclusion, which gradually disappeared in the alloy due to buoyancy force. On the other hand, when (pct $Fe_tO)_0$ = 15, [pct. T. O] first increased, showed a maximum, then decreased. This was followed by a minimum in the [pct. T. O], then [pct. T. O] increased again. There should have been the following reaction:

$$(FeO) = Fe + \underline{O} \quad (2)$$

and the $\underline{O}$ can be attributed to the increase of [pct. T. O]. Indeed, N_A, the measured inclusion number density by FE-SEM, showed different behavior to that of [pct. T. O]. Therefore, the measured [T. O] after passing the minimum in the [pct. T. O] is likely to correspond to soluble O content. It is evident that increasing (pct $Fe_tO)_0$ increased O content in the liquid alloy, and this results in "reoxidation" in the liquid steel. Other cases (B5, B10, B15, C5, C10, C15) were also similar (Cho, Cha, and Kang, 2021). Now, the task is to understand how the slag composition (C/A, (pct $Fe_tO)_0$) influences the reoxidation reaction rate.

REOXIDATION KINETICS MODEL

The reoxidation reaction rate was represented by a temporal change of [pct. S. Al], d[pct. S. Al]/dt, as the soluble Al is the reactant of the reoxidation reaction (Reaction (1)). Assuming that 1) local equilibrium at the slag-alloy interface is valid for Reaction (1), 2) mass balance in the system is kept thereby the change of the mass of slag components (FeO, Al_2O_3) can be calculated by the change of the mass of alloy components ([pct. S. Al]), the reaction rate could be formulated in two ways:

$$\frac{d[\text{pct.S.Al}]}{dt} = -\frac{A\rho_{\text{steel}}}{W_{\text{steel}}} k_{\text{Al}}^{\text{M}}\left([\text{pct. S. Al}] - [\text{pct. S. Al}]^i\right) \quad (3)$$

if the reoxidation reaction was only controlled by mass transport of Al (from bulk to the slag-alloy interface), or

$$\frac{d[\text{pct.S.Al}]}{dt} = -\frac{A\text{M}_{\text{Al}}}{W_{\text{steel}}} k_{\text{Al}-\text{Al}_2\text{O}_3}^{\text{app}} \left(\frac{\rho_{\text{steel}}}{\text{M}_{\text{Al}}}[\text{pct. S. Al}] - \frac{1}{L_{\text{Al}-\text{Al}_2\text{O}_3}} \frac{\rho_{\text{slag}}}{\text{M}_{\text{Al}_2\text{O}_3}} (\text{pct. Al}_2\text{O}_3)\right) \quad (4)$$

if the reoxidation reaction was only controlled by mass transport of Al and Al_2O_3 (from bulk to the slag-steel interface), simultaneously, where t, A, ρ_j, W_j, M_j, k_{Al}^{M}, and $L_{\text{Al}-\text{Al}_2\text{O}_3}$ are the reaction time, the reaction area (interfacial area between the slag and the alloy), the density of the phase j, the mass of the phase j, the atomic or molecular mass of j, the mass transport coefficient of Al in the alloy, and the distribution coefficient of Al between the alloy and the slag which is expressed as (Cho, Cha, and Kang, 2021):

$$L_{\text{Al}-\text{Al}_2\text{O}_3} = \frac{(\text{pct.Al}_2\text{O}_3)^i}{[\text{pct.S.Al}]^i} \frac{\rho_{\text{slag}}}{\rho_{\text{steel}}} \frac{\text{M}_{\text{Al}}}{\text{M}_{\text{Al}_2\text{O}_3}} \quad (5)$$

The superscript i means the "interface". The apparent rate constant for the mixed rate model in Eq. (4) is:

$$k_{\text{Al}-\text{Al}_2\text{O}_3}^{\text{app}} \equiv \frac{1}{k_{\text{Al}}^{\text{M}}} + \left(\frac{1}{2L_{\text{Al}-\text{Al}_2\text{O}_3}}\right) \frac{1}{k_{\text{Al}_2\text{O}_3}^{\text{S}}} \quad (6)$$

where $k_{\text{Al}_2\text{O}_3}^{\text{S}}$ is the mass transport coefficient of Al_2O_3 in the slag. As was proposed by Kim and Kang (Kim and Kang, 2018), the mass transport coefficient of Al_2O_3 in slag phase was assumed to be inversely proportional to viscosity of the slag:

$$k_{\text{Al}_2\text{O}_3}^{\text{S}} = k_{\text{Al}_2\text{O}_3}^{\text{S},^\circ} \times \frac{\eta}{\eta^\circ} \quad (7)$$

where η is the viscosity of the slag, and $k_{\text{Al}_2\text{O}_3}^{\text{S},^\circ}$, and η° are the mass transport coefficient of Al_2O_3 and the viscosity of a reference slag. k_{Al}^{M} and $k_{\text{Al}_2\text{O}_3}^{\text{S},^\circ}$ were optimized by fitting the experimental data to the model equation. It should be noted that the Eq. (4) contains the interfacial concentration terms *via* $L_{\text{Al}-\text{Al}_2\text{O}_3}$, which varies during the reaction. The interface compositions ([pct. S. Al]^i and (pct. $Al_2O_3)^i$) also vary during the reaction and those can be calculated using CALPHAD approach without assuming the volume or thickness of the interface reaction zone. Detailed procedure to obtain the interface compositions and subsequent steps to calculate $L_{\text{Al}-\text{Al}_2\text{O}_3}$, $k_{\text{Al}-\text{Al}_2\text{O}_3}^{\text{app}}$, and d[pct. S. Al]/dt can be found in the present authors' article (Cho, Cha, and Kang, 2021).

REOXIDATION KINETICS ANALYSIS

FIG 2 shows the extent of the reoxidation by temporal change of the normalized soluble Al content in the logarithmic scale (log [pct. S. Al]/[pct. S. Al]$_0$) (Cho, Cha, and Kang, 2021). Closed symbols are the measured data. Increasing (pct. $Fe_tO)_0$ from 5 to 15 (from bottom panel to top panel) decreased [pct. S. Al] faster, therefor the reoxidation occurred faster.

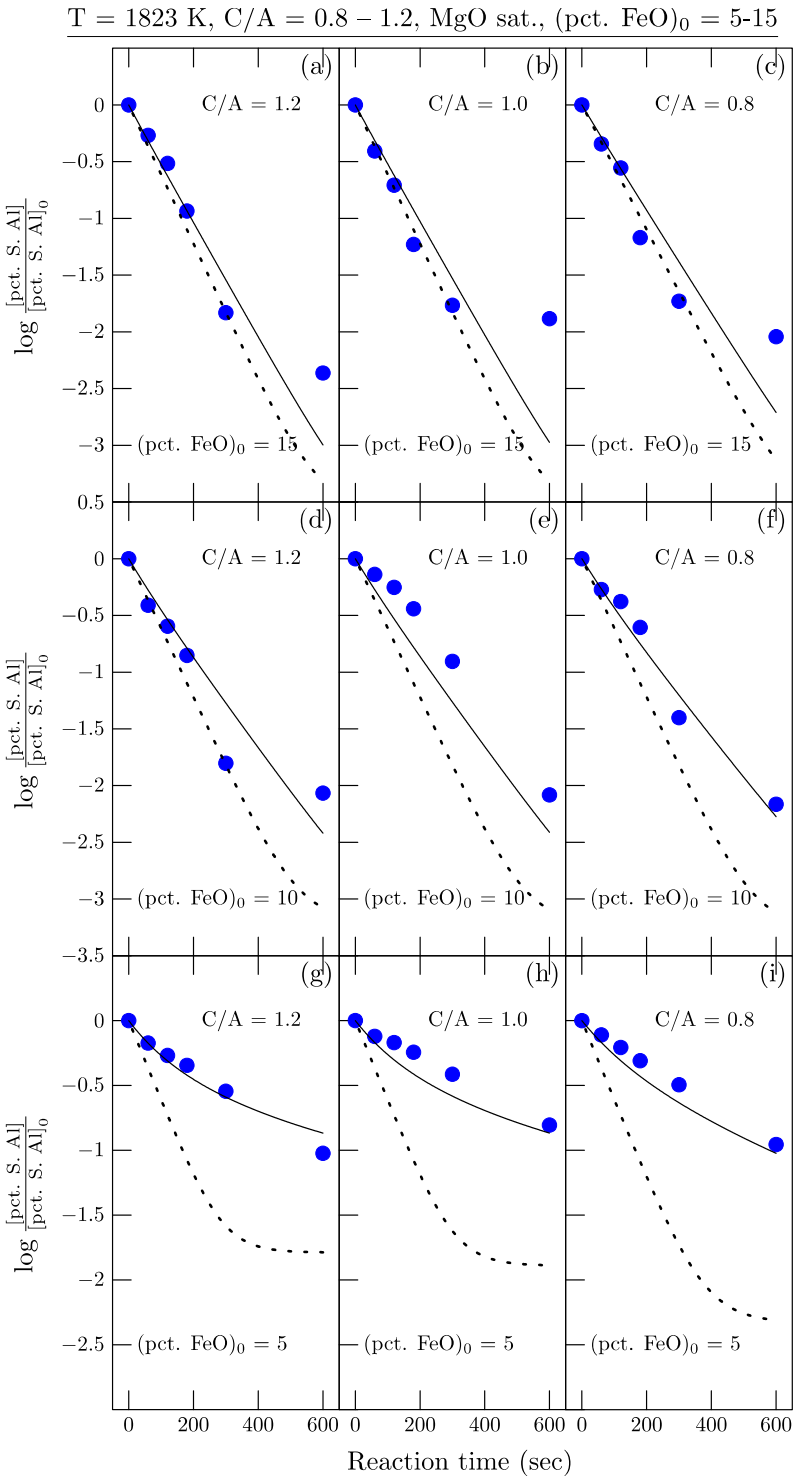

FIG 2 – Comparison between the experimental data and the model calculations for log [pct. S. Al]. Symbols are the experimental data, the dotted lines from Eq. (3) assuming the single rate controlling mechanism, and the solid lines from Eq. (4) assuming the mixed rate controlling mechanism (Cho, Cha, and Kang, 2021).

The dotted lines were the calculated extent of the reoxidation by Eq.(3), assuming the reoxidation was exclusively controlled by the mass transport of Al in the steel only. It was reasonable when (pct.

$Fe_tO)_0$ was high (15), but deviated gradually from the experimental data as (pct. $Fe_tO)_0$ decreased. The lower (pct. $Fe_tO)_0$ means the higher viscosity of the slag. This suggests that the mixed controlling concept formulated by Eq. (4) would be adequate. After a series of calculations, k_{Al}^{M} and $k_{Al_2O_3}^{S,\circ}$ were optimized by fitting the experimental data to the model equation. The solid lines are the calculated extent of the reoxidation by Eq.(4) in the context of the mixed controlling rate. A good agreement was achieved. It should be stressed that the extent of the reoxidation in view of the experiment and the model calculations does not clearly suggest the role of C/A on the reoxidation.

The developed model was manipulated to extract the reaction mechanism. The extent of reoxidation by Eq. (4) requires $k_{Al-Al_2O_3}^{app}$ and $L_{Al-Al_2O_3}$, and these two properties require the property at the interface [pct. S. Al]^i. FIG 3 shows the calculated [pct. S. Al]^i, $L_{Al-Al_2O_3}$, and $k_{Al-Al_2O_3}^{app}$ for the nine slag samples (numbers near the curly bracket means (pct. $Fe_tO)_0$).

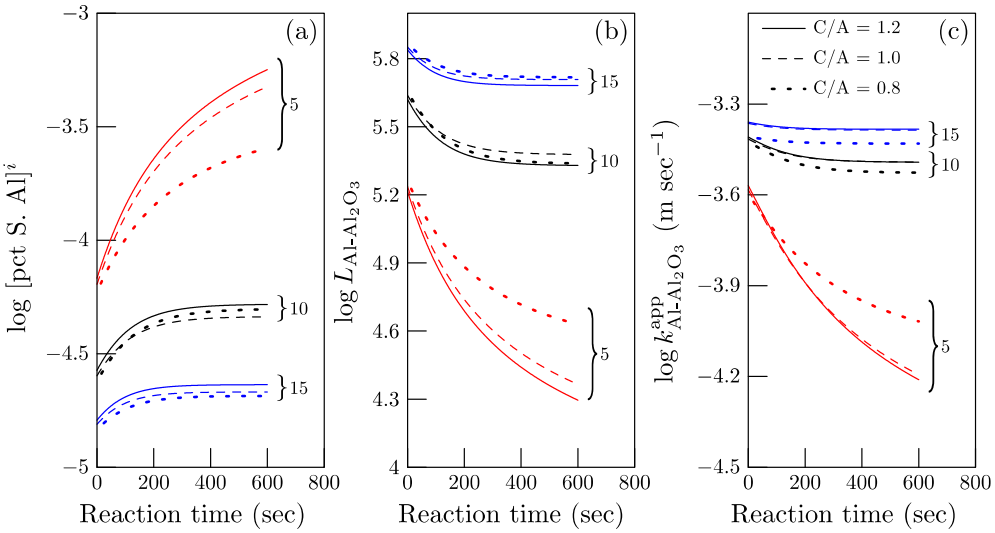

FIG 3 – Calculated various properties from during the reoxidation reaction at 1550 °C: (a) [pct. S. Al]^i, (b) $L_{Al-Al_2O_3}$, and (c) $k_{Al-Al_2O_3}^{app}$ (Cho, Cha, and Kang, 2021).

The three properties depend on *t*, (pct. $Fe_tO)_0$, and C/A. In general, as the reoxidation proceeded, soluble Al at the interface increased, thereby decreasing the driving force of the reaction. This is reflected in the decrease in the Al distribution ratio, inducing a lower driving force. This lowers the apparent rate constant, and finally, the reoxidation reaction ceased to proceed further. It should be stressed that the apparent rate constant is indeed not a constant, but varies during the reaction.

(pct. $Fe_tO)_0$. is the most dominant factor in the control of the reoxidation rate. When (pct. $Fe_tO)_0$ is high, the C/A ratio is not a critical factor in the three properties in FIG 2. However, at the lower (pct. $Fe_tO)_0$ = 5, C/A ratio does influence the three properties: increasing C/A ratio increased [pct. S. Al]^i and decreased $L_{Al-Al_2O_3}$ and $k_{Al-Al_2O_3}^{app}$. Therefore, increasing C/A ratio would decrease the reoxidation rate. High C/A ration decreased the reoxidation rate because $L_{Al-Al_2O_3}$ is low, which is due to high [pct. S. Al]^i. At the slag-steel interface, [pct. S. Al]^i is determined by the equilibrium of Reaction (1). It is known that increasing C/A in the $CaO-Al_2O_3-Fe_tO$ slag lowers the activity of Fe_tO at the same (pct. Fe_tO). This results in a higher soluble Al content. Although the slag used in the present study and RH slags in practical operations contain some other minor components such as MgO, increasing C/A ratio in RH slag of low (pct. $FeO)_0$ (*i.e.* ~5) can lower the reoxidation rate. This conclusion is in agreement with recent reports (Ji et al., 2018; Ji et al., 2020).

In practical RH slag operation, Fe_tO originates from BOF slag, introduced due to partial entrapment during tapping. Fe_tO is a major cause of reoxidation during RH processing. Deoxidizing the slag by eliminating Fe_tO using Al or C sources is a potential method to control reoxidation. However, reducing Fe_tO is challenging due to slag solidification and fume generation, impacting workability. Yet, higher Fe_tO aids in absorbing alumina inclusions, enhancing viscosity (Park et al., 2020).

Balancing Fe_tO content is crucial, considering reoxidation prevention versus viscosity benefits. Alternatively, killing Fe_tO and adding a non-reducible flux can achieve the same goal, but cost and refractory life become additional considerations.

CONCLUSIONS

In the investigation of ULC steel reoxidation during the RH process, an analysis of the reaction rate and mechanism was conducted through a series of laboratory-scale experiments and the utilization of a reaction rate model that integrates CALPHAD thermodynamics and mass transport theory (Cho, Cha, and Kang, 2021). The observed increase in reoxidation rate with higher initial percentages of Fe_tO ((pct. $Fe_tO)_0$) and the significance of variations in the C/A ratio were particularly notable when (pct. $Fe_tO)_0$ was low (5 in this study). The predominant influence on the reoxidation rate was found to be the mass transport of Al in liquid steel. However, as (pct. $Fe_tO)_0$ decreased, the rate-controlling step shifted towards mixed transport control, involving Al_2O_3 transport. A new reaction rate model was developed, incorporating local equilibrium through the CALPHAD method, mixed transport rate in both phases, and the viscosity effect on mass transport coefficients of Al_2O_3 or Fe_tO in the slag. This model demonstrated a good alignment with the experimental data. At high (pct $Fe_tO)_0$, the C/A ratio in the slag had minimal impact on the reoxidation rate. Conversely, at low (pct $Fe_tO)_0$, increasing C/A effectively reduced the reoxidation rate, showcasing its potential to suppress reoxidation.

ACKNOWLEDGEMENTS

This work was financially supported by POSCO, Rep. of Korea.

REFERENCES

Bale, C.W. *et al.* (2016) 'FactSage thermochemical software and databases, 2010–2016', *Calphad*, 54, pp. 35–53.

Cho, Y.-M., Cha, W.-Y. and Kang, Y.-B. (2021) 'Reoxidation of Al-killed ultra-low C steel by Fe_tO in RH Slag: experiment, reaction rate model development, and mechanism analysis', *Metallurgical and Materials Transactions B*, 52(5), pp. 3032–3044.

Feichtinger, S. *et al.* (2014) 'In situ observation of the dissolution of SiO_2 particles in $CaO–Al_2O_3–SiO_2$ slags and mathematical analysis of its dissolution pattern', *Journal of the American Ceramic Society*, 97(1), pp. 316–325.

Hong, H.-M. and Kang, Y.-B. (2021) 'Simultaneous analysis of soluble and insoluble oxygen contents in steel specimens using inert gas fusion infrared absorptiometry', *ISIJ International*, 61(9), pp. 2464–2473.

Ji, Y. *et al.* (2018) 'Effects of FeO and CaO/Al_2O_3 ratio in slag on the cleanliness of Al-killed steel', *Metallurgical and Materials Transactions B*, 49(6), pp. 3127–3136.

Ji, Y. *et al.* (2020) 'Oxygen transfer phenomenon between slag and molten steel for production of IF steel', *Journal of Iron and Steel Research International*, 27, pp. 402–408.

Kim, M.-S. and Kang, Y.-B. (2018) 'Development of a multicomponent reaction rate model coupling thermodynamics and kinetics for reaction between high Mn-high Al steel and $CaO-SiO_2$-type molten mold flux', *Calphad*, 61, pp. 105–115.

Park, Y. *et al.* (2020) 'Dissolution kinetics of alumina in molten $CaO–Al_2O_3–Fe_tO–MgO–SiO_2$ oxide representing the RH slag in steelmaking process', *Journal of the American Ceramic Society*, 103(3), pp. 2210–2224.

Park, J.-H and Kang, Y.-B. (2023) `Reoxidation phenomena of liquid steel in secondary refining and continuous casting Processes – A Review', *steel research international*, https://doi.org/10.1002/srin.202300598.